JOURNAL OF MATERIALS SCIENCE 14 (1979) 2225–2235

# Residual stress effects in sharp contact cracking

## Part 2 *Strength degradation*

D. B. MARSHALL, B. R. LAWN, P. CHANTIKUL
*Department of Applied Physics, School of Physics, University of New South Wales, N.S.W. 2033, Australia*

A detailed strength analysis for brittle surfaces containing dominant flaws produced under elastic–plastic indentation loading is presented. The condition for failure is formulated in terms of stress intensity factors representing driving forces associated with applied tension and residual indentation fields. Incorporation of the second of these components depresses the equilibrium applied stress–crack size function; this depression is accentuated at small crack size, such that the function passes through a maximum. Depending on the relative intensity of the residual indentation field, the starting size of the median cracks, as determined from Part 1 of this study, may lie on either side of this maximum: "large" cracks, i.e. those starting beyond the maximum, fail spontaneously from an unstable branch of the applied stress curve; "small" cracks undergo precursor stable growth to a critical depth at the stress maximum before failing. Observations of median crack growth in annealed and tempered soda-lime glass discs taken to failure in biaxial flexure confirm the existence of an energy barrier to crack instability. The important implications of these manifestations of the residual indentation field in predicting strength degradation characteristics for prospective adverse contact conditions are discussed for test pieces subjected to various imposed surface stress states.

## 1. Introduction

Part 1 of this study described the role of residual stress effects in the evolution of median fracture beneath sharp indenters [1]. In particular, we noted the potential continuation of crack growth during the unloading half-cycle of an indentation event, and the persistence of a crack driving force on completion of this event. With the recent development of indentation based theories of contact-induced strength degradation for brittle surfaces [2 to 11], it is of some importance to investigate how such effects might manifest themselves in the response to a subsequent tensile stress field. Whilst the *existence* of residual stress terms in the strength degradation equations has been previously acknowledged, their full *significance* has been obscured by the special procedures adopted to "calibrate" the indentation fracture parameters which appear in the formulation [6, 11]. Of special concern in this connection is the calibration of an "effective" critical stress intensity factor for the test material: indentation–strength data yield a value which tends to lie some 30% below that determined by more conventional fracture testing techniques. This means that any attempt to predict strength degradation characteristics from first principles, using established material parameters, is liable to systematic discrepancy.

In this paper we modify the earlier degradation analyses for sharp indenters by incorporating residual stress terms into the strength equations. We shall concentrate on crack growth under equilibrium conditions, notwithstanding the fact that residual stress effects may well be even more deleterious in kinetic fracture [12]. Since much handling damage on brittle surfaces may have its origins in contact events closely resembling the sharp-indenter configurations described in Part 1, the implications of the present work could be

0022–2461/79/092225–11 $03.10/0  

expected to extend to more general theories of strength based on flaw characteristics.

## 2. Incorporation of residual-stress terms into strength equations

Consider now the indentation–failure sequence of Fig. 1. In Fig. 1a a sharp indenter produces penny-like median cracks, in the manner described in Part 1. It is possible that under the combined action of the indentation load $P$ and some appropriate surfaces stress $\sigma_s$ the test piece may fail spontaneously during the contact event [11]. If it survives the contact, the degraded test surface is subject to premature failure during subsequent service. In the latter case the characteristic radius $c_0$ of the starting penny like flaw which determines the ultimate strength may be identified with the indentation crack size, i.e. either $c^*$ or $c^\dagger$, whichever is the larger [1]. A complete description of strength degradation characteristics therefore requires an analysis of median crack response in an applied tension field $\sigma_a$, Fig. 1b. Our aim in this section will be to fulful this requirement.

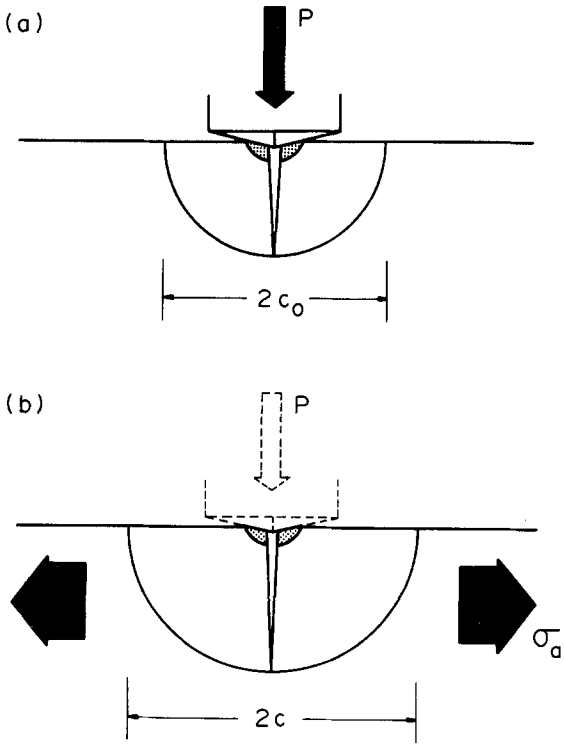


*Figure 1* Indentation–failure model. (a) Vickers indenter at normal load produces median crack flaw system of characteristic dimension $c_0$; (b) cracks extend to dimension $c$ under combined action of residual indentation field (represented here by "ghost" contact) and applied tensile stress $\sigma_a$. Surface stresses (not shown) may also drive the cracks.

As in Part 1, we determine the net mechanical force on the fracture system in terms of additive stress intensity factors. Even before application of the tensile field in Fig. 1b the median cracks experience a residual driving force from the preceding indentation event, as defined by the term

$$K_r = \chi_r P^*/c^{3/2}, \tag{1}$$

with $P^*$ the peak contact load and $\chi_r$ the associated indenter–specimen constant. Superposition of the tension $\sigma_a$ over the crack area gives rise to the contribution

$$K_a = \sigma_a(\pi\Omega c)^{1/2}, \tag{2}$$

where $\Omega$ is a crack geometry constant. Finally, if the cracks are simultaneously subjected to a uniform surface stress $\sigma_{s'}$, we have a third term,

$$K_{s'} = \sigma_{s'}(\pi\Omega c)^{1/2}; \tag{3}$$

surface stresses may be present in both the indentation and strength tests (e.g. tempered surfaces, $\sigma_s = -\sigma_R = \sigma_{s'}$), or in indentation only (e.g. surfaces under reversible pre-stress, $\sigma_s \neq 0$, $\sigma_{s'} = 0$).

For equilibrium crack growth the net stress intensity factor remains constant at a critical level, i.e.

$$K = K_r + K_a + K_{s'} = K_c. \tag{4}$$

Equations 1 to 3 combine with Equation 4 to give

$$\chi_r P^*/c^{3/2} + \sigma_a(\pi\Omega c)^{1/2} + \sigma_{s'}(\pi\Omega c)^{1/2} = K_c. \tag{5}$$

An applied stress–crack size relation follows by straightforward transformation:

$$\sigma_a = [K_c/(\pi\Omega c)^{1/2}]\,(1 - \chi_r P^*/K_c c^{3/2}) - \sigma_{s'}. \tag{6}$$

The strength, $\sigma$, is then defined as the value of $\sigma_a$ at which the crack propagates spontaneously without limit. We may note that Equation 6 reduces to the standard strength relation, $\sigma \propto K_c c^{-1/2}$, as $\chi_r \to 0$, i.e. as the residual stress effect disappears.

In order to avoid having to specify $\sigma_{s'}$ at this stage it is convenient to define a "stress function"

$$\mathscr{S}(c) = \sigma_a + \sigma_{s'}. \tag{7}$$

We may show from Equation 6 that this function has a maximum at

$$\mathscr{S}_m = 3K_c/4(\pi\Omega c_m)^{1/2} \quad (8a)$$

$$c_m = (4\chi_r P^*/K_c)^{2/3} \quad (8b)$$

and may accordingly be expressed in the "universal", normalized form

$$\mathscr{S}/\mathscr{S}_m = \tfrac{1}{3}(c_m/c)^{1/2}[4-(c_m/c)^{3/2}]. \quad (9)$$

An appropriate plot is given in Fig. 2. The stability of crack extension in the applied field is now seen to depend on the relative values of $c_0$ and $c_m$. For $c_0 > c_m$, the crack system becomes unstable at $\mathscr{S} = \mathscr{S}(c_0)$, e.g. path 1; the strength is then given directly by Equation 7 with $\sigma = \sigma_a$ at $c = c_0$, i.e.

$$\sigma = \mathscr{S}(c_0) - \sigma_{s'} \quad (c_0 > c_m). \quad (10a)$$

For $c_0 \leqslant c_m$, however, the crack must first overcome an energy barrier to failure by growing stably until $\mathscr{S} = \mathscr{S}_m$, path 2; the strength in this case is given by $\sigma = \sigma_a$ at $c = c_m$, i.e.

$$\sigma = \mathscr{S}_m - \sigma_{s'} \quad (c_0 \leqslant c_m). \quad (10b)$$

Thus, whereas the starting flaw size assumes a controlling role in Equation 10a, the only way it enters into Equation 10b is via the inequality expressing the condition of validity. In this context it is seen from Equation 8b that the prospect of precursor stable growth in a strength test increases with the value of $\chi_r$.

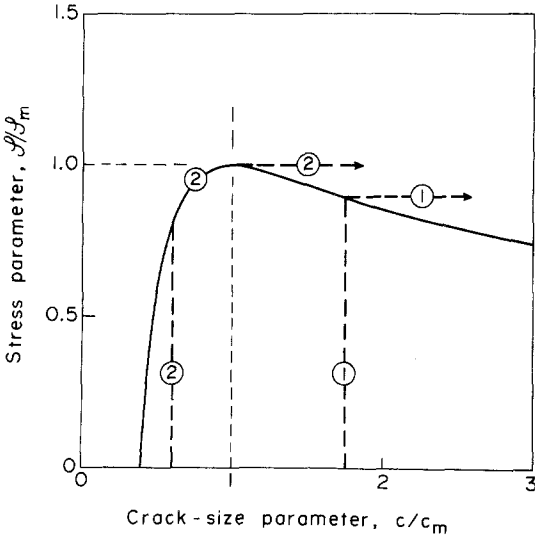


*Figure 2* Plot of function Equation 9. Path 1 illustrates the spontaneous failure mode for flaws in the range $c_0 > c_m$, path 2 the activated mode involving precursor stable growth for flaws in the range $c_0 \leqslant c_m$.

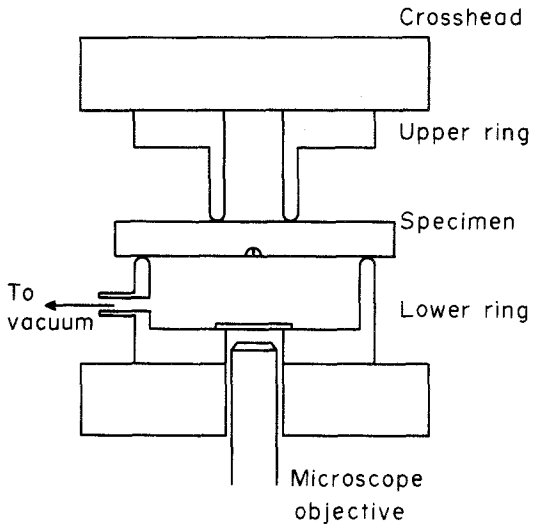


*Figure 3* Schematic of strength testing set up for following crack growth during application of tensile stress.

An explicit statement as to which of Equations 10a and b will determine the degradation characteristics for any given indenter–specimen system requires an evaluation of $c_0$ via the formulation of Part 1. Before attempting any such evaluation, however, we may usefully examine some of the essential predictions of the strength analysis by observing crack growth directly in our model soda-lime glass system [1].

## 3. Observations of crack growth during strength testing

The simple experimental setup shown in Fig. 3 allowed direct monitoring of the indentation flaws during application of the tensile field in the strength test. Discs, ≈ 50 mm diameter and 3 mm thickness, of the same glass used in Part 1, were first indented with a Vickers pyramid at a maximum load $P^* = 50$ N. These were then stressed biaxially in a symmetrical ring-on-ring arrangement [6], with the contact flaw on the tension side. The small volume enclosed by the disc test surface and the lower ring assembly was either flushed continuously with dry nitrogen or evacuated (≈ 1 mPa) during stressing; the discs were, of course, exposed to the atmosphere in the preceding transferral from the indentation to the strength testing equipment, an operation carried out usually in less than 30 min. An inverted microscope with a constant-interval, motor-driven camera attachment was used to photograph the radially expanding median cracks. The applied stress level was evaluated, via simple plate theory [13], in terms of the flexural loading, with due

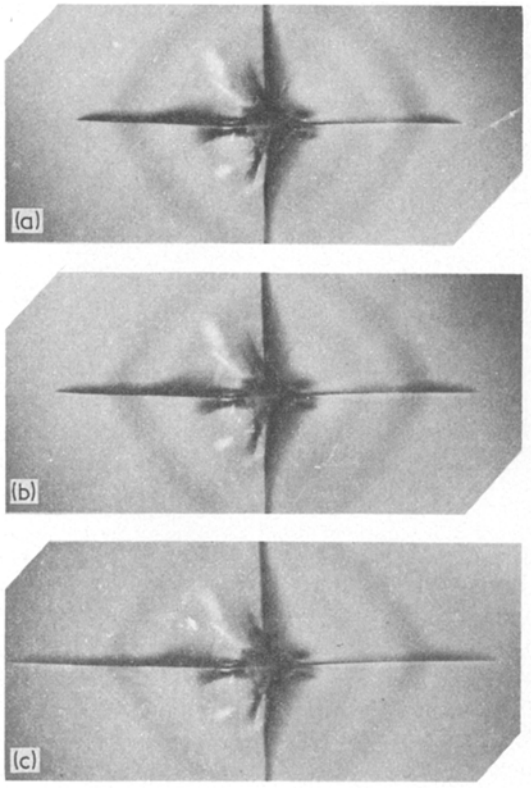


*Figure 4* Growth of median crack in annealed soda-lime glass ($\sigma_s = 0 = \sigma_{s'}$) leading to failure in strength test, dry $N_2$ conditions: (a) $\sigma_a = 0$, (b) $\sigma_a = 28.3$ MPa, (c) $\sigma_a = 31.5$ MPa. Starting crack from Vickers indentation, $P^* = 50$ N. (Faintly visible lateral cracks do not extend during test.) Width of field 1020 $\mu$m.

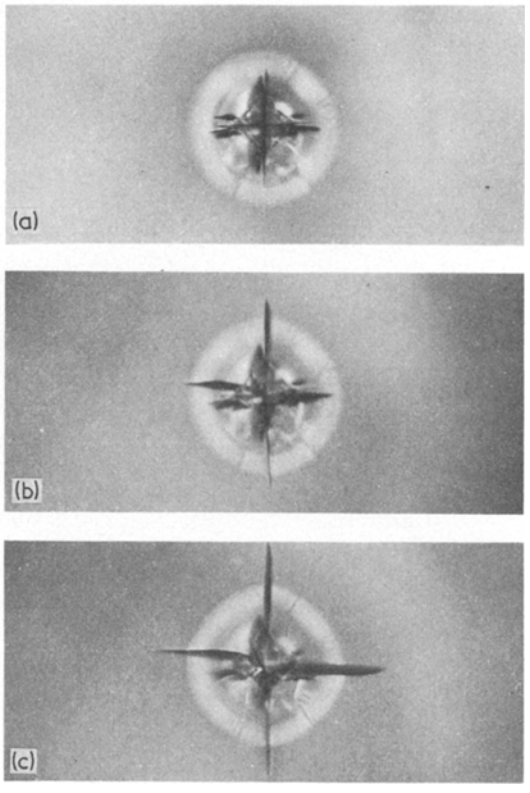


*Figure 5* Growth of median crack in tempered soda-lime glass ($\sigma_s = -\sigma_R = -128$ MPa $= \sigma_{s'}$) leading to failure in strength test, dry $N_2$ conditions: (a) $\sigma_a = 0$, (b) $\sigma_a = 143$ MPa, (c) $\sigma_a = 170$ MPa. Starting crack from Vickers indentation, $P^* = 50$ N. (Lateral cracks do not extend during test.) Width of field 1020 $\mu$m.

allowances for any pressure differences across the plate surfaces.

Photographic sequences of crack response during stressing to failure are shown in Figs. 4 and 5 for indentations on annealed ($\sigma_{s'} = 0$) and tempered ($\sigma_{s'} = -128$ MPa) surfaces. Considerable subcritical extension is evident. In order to verify that this extension occurred under the conditions of stable equilibrium envisaged in Section 2 and not according to some kinetic process, some dummy runs were made with halt points in the stress–time loading characteristics. Dimensions $c$ were measured as in Fig. 1b on only one of the orthogonal median cracks, that which led to failure of the plate. Typical data are shown in Figs. 6 and 7. There is a tendency for the crack growth to overshoot the stress halt points in the annealed glass, indicating that non-equilibrium effects are not entirely absent. However, the extent of growth during the halt periods is dwarfed by that during the stress rise time. Moreover, in the tempered glass, which generally has a lower susceptibility to kinetic fracture [4], this crack overshoot tendency could not be detected, within the limits of experimental accuracy, at all. It is concluded that the role of slow crack growth is secondary to that of stable equilibrium growth in the conditions of strength testing used in this work.*

The results of experimental runs investigating the relation between applied stress and crack size are plotted as the data points in Figs. 8 and 9 for

*More detailed, numerical calculations of crack response under the test conditions pertaining to Figs. 6 and 7, using Equations 1 to 4 in conjunction with the crack velocity data of Wiederhorn *et al.* for soda-lime glass in vacuum [15], confirm that the overshoot is consistent with intrinsic slow crack growth. Similar calculations in the absence of halt points show that the kinetic contribution amounts to less than 3% of the total crack extension observed as failure.

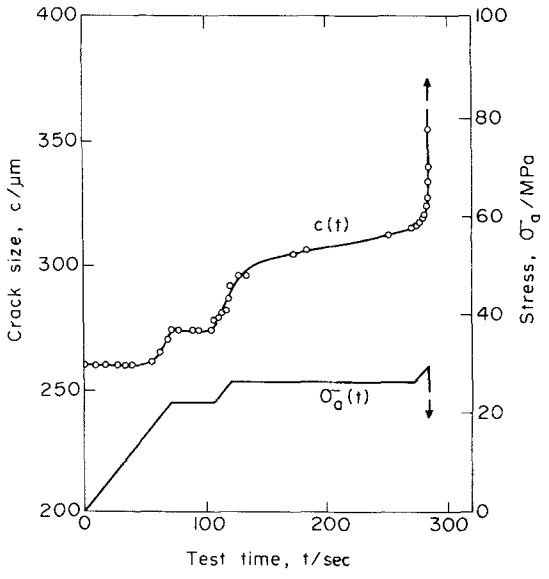


*Figure 6* Time variation of applied stress and crack size in vacuum strength test on annealed glass.

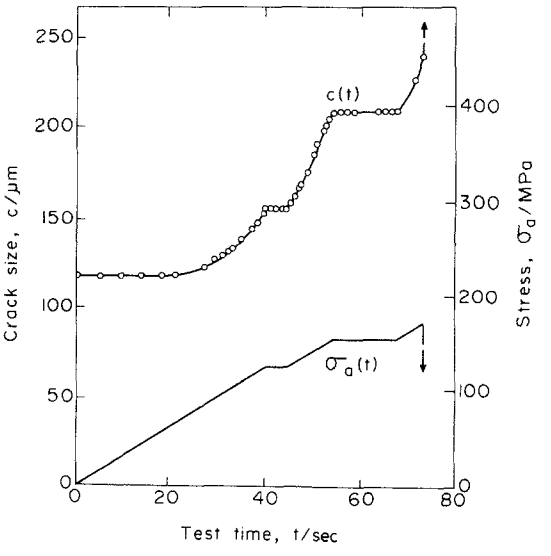


*Figure 7* Time variation of applied stress and crack size in vacuum strength test on tempered glass.

annealed and tempered glass respectively. No significant differences were noted between tests run in dry nitrogen and vacuum. Most of the runs were conducted on as-indented surfaces, but in the case of Fig. 8 three specimens were re-annealed after indentation to remove the residual stress field about the contact site. As a safeguard against the possibility that such re-annealing may have caused some crack-tip blunting, the flexural stress was initially applied in laboratory atmosphere until a small amount of slow crack growth was detected; then inert environmental conditions were restored for the remainder of the loading to failure (cf. Appendix, Part 1). The full curves in Figs. 8 and 9 are the appropriate theoretical predictions of Equation 6, using $K_c = 0.75$ MPa $m^{1/2}$, $\Omega = 0.30$ and $\chi_r = 0.026$ (as-indented) or $\chi_r = 0$ (re-annealed). Notwithstanding certain systematic discrepancies between theory and experiment, we may draw the following conclusions for the glass under study here:

(i) The relatively small subcritical crack growth prior to failure of the re-annealed surfaces in Fig. 8 reinforces our earlier conclusion con-

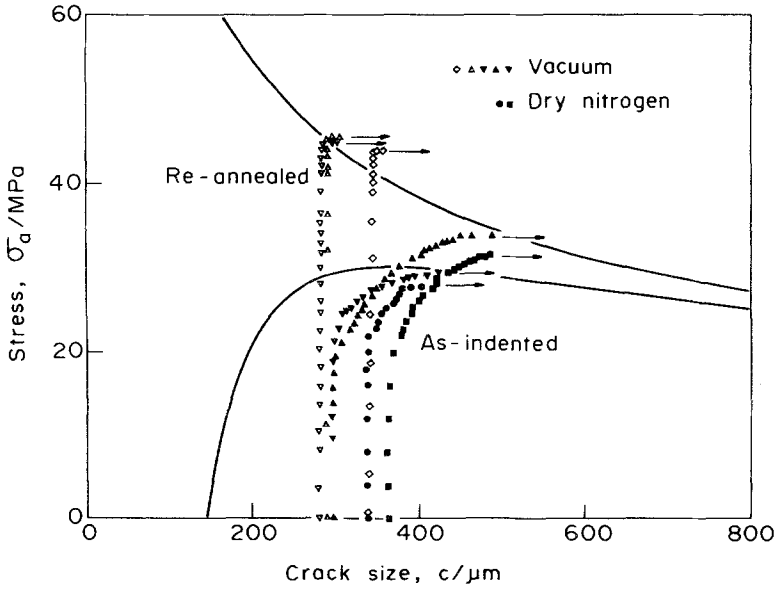


*Figure 8* Crack response in strength tests on annealed soda-lime glass in vacuum or dry nitrogen. Arrows designate failure condition $\sigma = \sigma_a$ at onset of unstable equilibrium. Specimens tested either as-indented (closed symbols) or re-annealed after contact (open symbols), with each symbol representing different run. Starting crack from Vickers indentation, $P^* = 50$ N. Stress rate $\dot{\sigma}_a = 3.2$ MPa $sec^{-1}$.

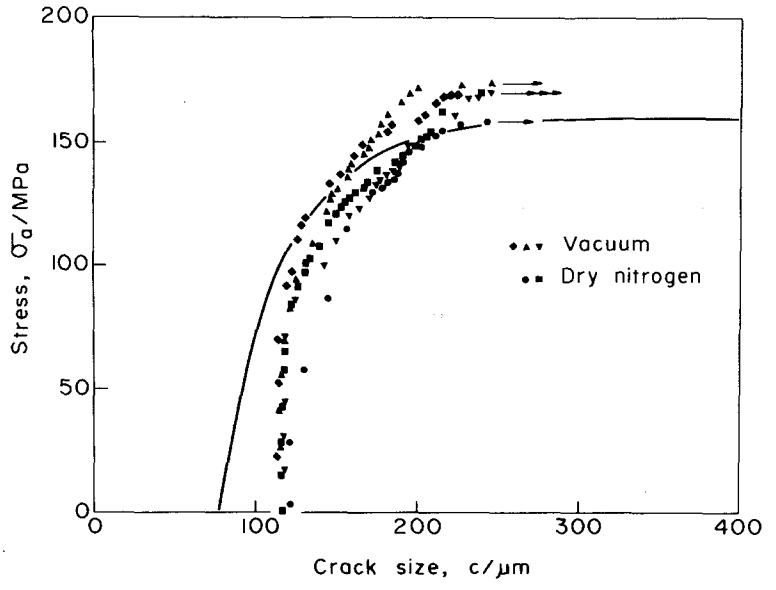


*Figure 9* Crack response in strength tests on tempered glass ($\sigma_R$ = 128 MPa) in vacuum and dry nitrogen. Arrows designate failure condition. Specimens tested as-indented, with each symbol representing different run. Starting crack from Vickers indentation, $P^*$ = 50 N. Stress rate $\dot{\sigma}_a$ = 30 MPa sec$^{-1}$.

cerning the minor role of kinetic effects in the strength determination.

(ii) Conversely, the relatively large extent of subcritical growth shown by the as-indented surfaces confirms the existence of significant residual-stress components in the crack driving forces, and, in particular, the attendant existence of an energy barrier to failure.

(iii) The sign of the residual stress component is such as to cause a general lowering of strength.

(iv) The tempered surface is stronger than the annealed surface by an amount approximately equal to the surface compression, in accordance with Equation 10b.

## 4. Implications in strength degradation

We now derive relations for the degraded strength of brittle surfaces in terms of the load delivered in sharp contact, as in Fig. 1, and compare the predicted degradation characteristics with experimental observations. We confine our attention here to contact conditions of sufficient severity that the indentation crack constitutes the dominant flaw in the specimen, mindful that there will be a low-load cut-off in the degradation [9]. A number of interesting contact configurations, according to surface stress states $\sigma_s$ and $\sigma_{s'}$, will be analysed, with particular attention paid in each case to the role of residual stress terms.

### 4.1. Theoretical derivations

It is necessary now to recall the equilibrium indentation equations given as Equation 7 in Part 1 [1]:

$$\chi_e P/c^{3/2} + \chi_r P/c^{3/2} + \sigma_s(\pi\Omega c)^{1/2} = K_c \quad (P\uparrow) \tag{11a}$$

$$\chi_e P/c^{3/2} + \chi_r P^*/c^{3/2} + \sigma_s(\pi\Omega c)^{1/2} = K_c \quad (P\downarrow). \tag{11b}$$

#### 4.1.1. Stress-free surfaces ($\sigma_s = 0 = \sigma_{s'}$)

Consider an annealed test piece to be subjected to the loading sequence of Fig. 1, free of any extraneous surface stresses. In this case we have, from Part 1, that the characteristic size of the equilibrium indentation crack at maximum contact, $c^*$, is greater than at complete unload, $c^\dagger$; it is therefore the former which determines the size of the starting flaw in the subsequent uniform tension loading. Putting $\sigma_s = 0$, $P = P^*$ into Equation 11a thus gives

$$c_0 = c^* = [(\chi_e + \chi_r)P^*/K_c]^{2/3}. \tag{12}$$

Comparison of this relation with Equation 8b then leads to

$$c_0/c_m = [(1 + \chi_e/\chi_r)/4]^{2/3}. \tag{13}$$

The critical condition $c_0 = c_m$ which distinguishes between failure paths of types 1 and 2 in Fig. 2 may now be restated as $\chi_r/\chi_e = 1/3$. Accordingly, when $c_0 > c_m$, the test piece fails spontaneously under the tensile loading in the manner of path 1, i.e. with $\sigma = \sigma_a$ at $c = c_0 = c^*$

and $\sigma_{s'} = 0$ in Equation 6, so that, with Equation 12, we have

$$\sigma = \{\chi_e^3 K_c^4/(\chi_e + \chi_r)^4(\pi\Omega)^{3/2}\}^{1/3}/P^{*1/3} \quad (\chi_r/\chi_e < 1/3). \tag{14a}$$

Alternatively, when $c_0 \leqslant c_m$, stable crack growth precedes failure in the manner of path 2, i.e. with $\sigma = \sigma_a = \sigma_m$ at $c = c_m$ and $\sigma_{s'} = 0$ in Equation 6; recourse to Equation 8b then gives

$$\sigma = \{27K_c^4/256\chi_r(\pi\Omega)^{3/2}\}^{1/3}/P^{*1/3} \quad (\chi_r/\chi_e \geqslant 1/3). \tag{14b}$$

It may be noted that the simple power relation, $\sigma P^{*1/3} =$ constant, applies in both cases, the difference in the two proportionality constants being determined uniquely by the $\chi$ parameters. We may also note that in the limit of $\chi_r \to 0$, Equation 14a necessarily applies, and with $\chi_e \to \chi$, reduces to an earlier degradation formulation [9].

### 4.1.2. Pre-stressed surface taken to failure during contact ($\sigma_s > 0$)

Consider now a situation similar to that described in section 4.1.1, but this time with the tensile stress responsible for failure acting *simultaneously with* rather than *subsequent to* the indentation event (in this case, of course, there is no need to specify any stress state $\sigma_{s'}$) [11]. The function $[P(c)]_{\sigma_s}$ transformed from Equation 11a passes through a maximum at $(\partial P/\partial c)_{\sigma_s} = 0$, i.e. at

$$c_c = [4(\chi_e + \chi_r)P_c/K_c]^{2/3} = 9K_c^2/16\pi\Omega\sigma_s^2, \tag{15}$$

which accordingly represents a critical crack depth for failure*. It may be noted that the same result is obtained by evaluating the maximum at $(\partial\sigma_s/\partial c)_P = 0$ for the transformed function $[\sigma_s(c)]_P$, i.e. the failure point is independent of loading path. In this latter case the crack size prior to application of the stress $\sigma_s$ is given by Equation 12, whence, with $P_c = P^*$ in Equation 15, we have $c_0/c_c = 1/4^{2/3}$: This simply confirms that stable crack growth must precede failure in this mode. Substitution of Equation 15 into Equation 11a to determine the failure condition $\sigma = \sigma_s$ at $c = c_m$ leads to

$$\sigma = \{27K_c^4/256(\chi_e + \chi_r)(\pi\Omega)^{3/2}\}^{1/3}/P_c^{1/3}. \tag{16}$$

This equation has the same form as the earlier strength degradation equation (Equation 14b), reflecting the common requirement of an energy barrier to failure; the present configuration is seen to be potentially more catastrophic, by an amount again determined uniquely by the $\chi$ parameters. Finally, we may duly acknowledge that if we replace $\chi_e + \chi_r$ with $\chi$, Equation 16 is equivalent to an earlier derivation [11].

### 4.1.3. Pre-stressed surface taken to failure after contact ($\sigma_s \neq 0$. $\sigma_{s'} = 0$)

In this case the surface in pre-stress survives the contact, and is taken to failure subsequently with the pre-stress removed. Relative to the situation described in Section 4.1.1 above, it might be expected that the effect of the superimposed stress $\sigma_s$ in the contact stage would be to depress or enhance the strength, depending on whether $\sigma_s$ be tensile or compressive. The possibility now exists that the median cracks may extend downward during indenter unloading, so we need to consider two alternatives for the starting flaw size $c_0$, namely $c^*$ or $c^\dagger$ (Section 2). First, when such downward extension does *not* occur, the pertinent crack dimension is $c^*$, given in implicit form by Equation 11a at $P = P^*$,

$$(\chi_e + \chi_r)P^*/c^{*3/2} + \sigma_s(\pi\Omega c^*)^{1/2} = K_c. \tag{17}$$

With the aid of Equation 8b, the critical condition $c^* = c_0 = c_m$ becomes $\chi_e/\chi_r = 3 - \Delta$, where

$$\Delta = \{256\chi_r(\pi\Omega)^{3/2}/K_c^4\}^{1/3}\sigma_s P^{*1/3}.$$

The critical ratio $\chi_r/\chi_e$ is therefore elevated above the stress free value 1/3 for $\sigma_s > 0$, and conversely diminished for $\sigma_s < 0$. In the region $c_0 > c_m$, putting $\sigma = \sigma_a$ at $c = c_0 = c^*$, $\sigma_{s'} = 0$, into Equation 6 does not lead to an explicit function $\sigma(P^*)$, making it necessary to resort to a numerical solution. However, for $c_0 \leqslant c_m$, Equation 6 with $\sigma = \sigma_a = \sigma_m$ at $c = c_m$, $\sigma_{s'} = 0$,

*Here we use a subscript $c$ in place of a superscript asterisk used in a previous paper [11] to denote the critical conditions – this is to distinguish from the alternative meaning of the asterisk notation adopted in the present work.

in conjunction with Equation 8b, reduces simply to

$$\sigma = \{27K_c^4/256\chi_r(\pi\Omega)^{3/2}\}^{1/3}/P^{*1/3} \quad [\chi_r/\chi_e \geqslant 1/(3-\Delta)]\,. \tag{18}$$

Comparison with the analogous expression Equation 14b for stress-free surfaces reveals an identical strength function $\sigma(P^*)$ – the existence of the energy barrier in the failure test washes out any prospective effect of the superimposed stress $\sigma_s$ on the ultimate strength. The only way $\sigma_s$ enters Equation 18 is via $\Delta$ in the conditional inequality; viewed in terms of Fig. 2, variations in $\sigma_s$ manifest themselves solely as lateral displacements of $c_0$ relative to $c_m$. Turning to the second possibility where downward crack extension *does* occur during indenter unloading, the pertinent starting crack dimension is $c^\dagger$ corresponding to $P = 0$ and $\sigma_s = 0$ in Equation 11b, i.e.

$$c_0 = c^\dagger = (\chi_r P^*/K_c)^{2/3}; \tag{19}$$

comparison with Equation 8b gives immediately $c_0/c_m = 1/4^{2/3}$; the condition $c_0 \leqslant c_m$ is therefore satisfied automatically in this case, whence Equation 18 is again applicable.

#### 4.1.4. Tempered surfaces ($\sigma_s = -\sigma_R = \sigma_{s'}$)

The analysis of Section 4.1.3 holds, with $-\sigma_R$ in place of $\sigma_s$ in the $\Delta$ term and, more importantly, since the surface compression persists in the strength test, with $-\sigma_{s'} = \sigma_R$ added to the right-hand side of Equation 18 in accordance with Equation 10.

### 4.2. Experimental data

We now investigate the level of agreement between the predictions of the above formulation and experimental degradation results. Thus in Figs. 10 to 12 the shaded bands, representing calculated strength characteristics, are to be compared with the data points. The calculations are based on the following parameters, evaluated for our glass in Part 1: $K_c = (0.75 \pm 0.05\,\text{MPa m}^{1/2}$, $\Omega = 0.30 \pm 0.08$, $\chi_e = 0.032 \pm 0.008$ and $\chi_r = 0.026 \pm 0.003$. The ratio $\chi_r/\chi_e = 0.81$ is sufficiently large to guarantee the existence of an energy barrier to failure under any of the surface stress conditions to be considered here. Our observations of precursor stable crack growth in the crack response plots of Figs. 8 and 9 confirm this, and demonstrate moreover that spurious slow crack growth during transfer of the specimens from the indentation to the strength testing apparatus is not great enough to cause the critical condition $c_0 = c_m$ to be exceeded. The results reported here were conducted in an inert oil environment, and as such may even more justifiably be regarded as pertaining to equilibrium fracture requirements.

Fig. 10 shows results for annealed glass tested as described in Sections 4.1.1 and 4.1.2 above. From Equations 16 and 14b, the degraded strengths with the indentation and applied stress fields acting simultaneously as compared to sequentially are in the ratio $[\chi_r/(\chi_e + \chi_r)]^{1/3} = 0.77$. This ratio will tend to unity for materials in which $\chi_r$ becomes the dominant indentation parameter; in this limit the indentation field intensity will not diminish on unloading, so it becomes irrelevant whether the failure stress is applied *during* or *after* the contact event. At the other extreme of $\chi_r \to 0$, comparison of Equations 16 and 14a shows this strength ratio to be 0.47, representing the maximum possible divergence between the two stressing configurations.

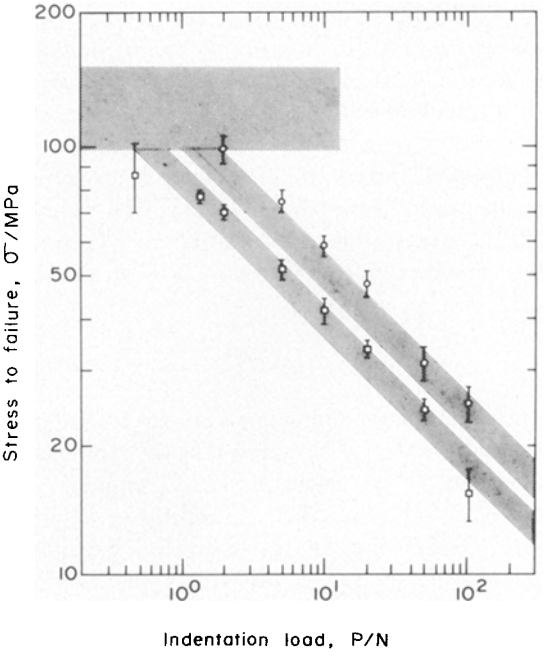


*Figure 10* Failure stress as function of contact load, for Vickers indentations on annealed soda-lime glass discs. Each data point represents mean and standard deviation of 8 to 10 tests. Lower results for tests with indentation and applied stress fields acting simultaneously, upper results for tests with same fields applied sequentially. Horizontal band is cut-off strength level determined by pre-present flaw distribution on as-received surfaces. Data after [11].

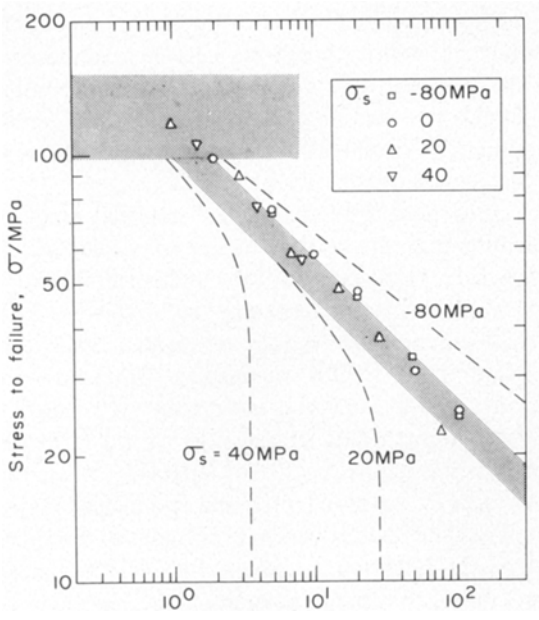


*Figure 11* Failure stress as function of contact load, for Vickers indentations on pre-stressed soda-lime glass discs. Each data point represents mean of 8 to 10 tests (error bars omitted – see Fig. 10 for typical values). Horizontal band is cut-off strength level determined by pre-present flaw distribution on as-received surfaces. Broken lines represent predicted degradation characteristics for purely elastic contact field.

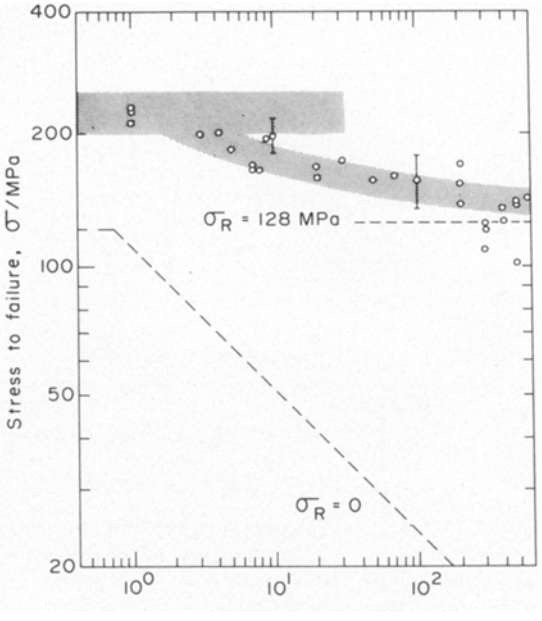


*Figure 12* Failure stress as function of contact load, for Vickers indentations on thermally tempered soda-lime glass discs. Data points represent individual tests, except those with error bars (mean and standard deviations of 8 to 10 tests). Horizontal band is cut-off strength level determined by pre-present flaw distribution on as-received surfaces. Data after [6].

The next set of results, Fig. 11, relates to the conditions of Section 4.1.3. In this plot the main, shaded band is the prediction of Equation 18 for all values of pre-stress $\sigma_s$ satisfying the inequality $\chi_r/\chi_e \geqslant 1/(3-\Delta)$. The data points are seen to confirm the predicted independence of $\sigma_s$. For comparison, degradation characteristics evaluated on the basis of a purely elastic contact are also plotted in Fig. 11, for each of the experimental values of $\sigma_s$: these evaluations are made in the manner outlined for the region $c_0 > c_m$ in Section 4.1.3, with $\chi_r = 0$ and $\chi_e = \chi$ adjusted to give a fit to the shaded line at $\sigma_s = 0$. It is evident that the observed results can only be explained in terms of a model which incorporates the residual stress effects.

Finally, we show in Fig. 12 some results for thermally tempered glass plate. Comparison of the results with the broken line representing $\sigma_{s'} = 0$ (from Fig. 11) demonstrates the strengthening that can be achieved by maintaining an internal surface compression $\sigma_R$ throughout the period of exposure to applied tensile fields.

In absolute terms, we may conclude that the modified degradation theory, in conjunction with the "calibration" procedures of Part 1 [1], is capable of predicting strength characteristics to within a typical scatter band of $\approx 10\%$.

## 5. Discussion

By incorporating residual stress effects into the indentation–strength fracture mechanics, we have established a basis for absolute predictions of the strength of brittle components under potentially degrading contact conditions. Whilst a model contact system has been used to illustrate the essential mechanics of strength degradation, the present analysis has general application. Thus, whereas our experimental data have been obtained on a specific soda-lime glass, there is nothing in the theory to preclude a similar analysis of other brittle materials, provided some care is taken to allow for possible effects of microstructural inhomogeneity and mechanical anisotropy. Again, although we have given explicit attention only to quasistatic loading conditions, extension to the practically important problem of sharp particle

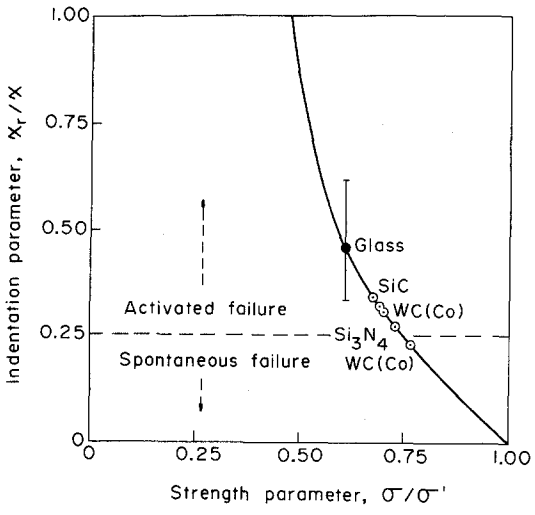


*Figure 13* Fractional component of indentation constant due to residual field, as function of as-indented–re-annealed strength ratio. Soda-lime glass datum, this work; other materials (including three WC–$C_0$ compositions), after [20].

impact can be readily made via an appropriate impulsive load–particle velocity relation [7]. The present equilibrium equations may also be used as a base for incorporating kinetic effects: although such effects are unlikely to influence events significantly in the relatively stable growth conditions of the indentation fracture cycle [16], they will certainly be expected to have important repercussions in the stressing to failure [12].

One particularly interesting outcome of the present strength formulation is the predicted existence of an energy barrier to failure in certain circumstances. As indicated in Section 2, the requirement for activation over such a barrier is that the median cracks be driven by the applied stress field to a depth $c_m$, in which case the initial depth $c_0$ no longer plays a part in the strength determination. This point has an important bearing on such questions as the relative susceptibilities to failure of components stressed *during* versus *after* the contact event (Fig. 10), or whether the surface stress history during service is likely to be a significant factor (cf. Figs. 11 and 12). As an example of the second question, we may cite the studies of Kirchner and Gruver on localized impact damage in pre-stressed ceramic plates [17–19]: these workers noted that the extent of contact cracking diminished as the surface pre-stress changed from tensile to compressive, and thence suggested that components should be designed with exposed surfaces in compression. The present work suggests that such suggestions should not be implemented without a careful appraisal of residual stress effects associated with the damage configuration.

It is in this context of an activated mode of failure that the relative values of $\chi_e$ and $\chi_r$ are specially pertinent. We have indicated in Part 1 how these parameters may be evaluated from fractographic observations of median crack evolution [1]. A less demanding procedure for achieving the same end is to make use of indentation–strength data of the type shown in Fig. 8, comparing the strengths of originally stress-free surfaces in the as-indented and re-annealed states. For as-indented surfaces, the degradation formulae given in Equation 14 are applicable; the corresponding formula for re-annealed surfaces may be derived in exactly the same way as Equation 14a, but with $\chi_r = 0$ in Equation 6, giving

$$\sigma' = \{K_c^4/(\chi_e + \chi_r)(\pi\Omega)^{3/2}\}^{1/3}/P^{*1/3}.$$

This relation, together with Equation 14, may be used to determine $\chi_r$ and $\chi_e$ without any need to measure crack dimensions. If we simply compare the two sets of formulae at a fixed value of $P^*$ we may derive expressions for the fractional component of the total indentation constant $\chi = \chi_e + \chi_r$ attributable to the residual field, noting that the critical condition $\chi_r/\chi_e = 1/3$ transforms to $\chi_r/\chi = 1/4$:

$$\chi_r/\chi = 1 - \sigma/\sigma' \qquad (\chi_r/\chi < 1/4)$$

$$\chi_r/\chi = (27/256)(\sigma'/\sigma)^3 \qquad (\chi_r/\chi \geqslant 1/4).$$

Failure may then be regarded as spontaneous in the range $0 \leqslant \chi_r/\chi < 1/4$, and activated in the range $1/4 \leqslant \chi_r/\chi \leqslant 1$. A plot of $\chi_r/\chi$ versus $\sigma/\sigma'$ is given in Fig. 13, together with data points representing relative strength measurements from several materials. It is apparent that the magnitude of the residual stress effect may vary considerably, emphasising the need to assess each individual material for prospective degradation resistant application on its own merits.

## Acknowledgements

This work was supported by the Australian Research Grants Committee.

## References


1. D. B. MARSHALL and B. R. LAWN, *J. Mater. Sci.* **14** (1979) 2001.
2. A. G. EVANS, *J. Amer. Ceram. Soc.* **56** (1973) 405.
3. B. R. LAWN and S. M. WIEDERHORN, *ibid.* **58** (1975) 428.
4. B. R. LAWN, E. R. FULLER and S. M. WIEDERHORN, *ibid.* **59** (1976) 193.
5. S. M. WIEDERHORN and B. R. LAWN, *ibid.* **60** (1977) 451.
6. D. B. MARSHALL and B. R. LAWN, *ibid.* **61** (1978) 21.
7. S. M. WIEDERHORN and B. R. LAWN, *ibid.* **62** (1979) 66.
8. B. R. LAWN, D. B. MARSHALL and S. M. WIEDERHORN, *ibid.* **62** (1979) 76.
9. B. R. LAWN and D. B. MARSHALL, "Fracture Mechanics of Ceramics", edited by R. C. Bradt, D. P. H. Hasselman and F. F. Lange (Plenum, New York, 1978) p. 205.
10. D. B. MARSHALL, B. R. LAWN, H. P. KIRCHNER and R. M. GRUVER, *J. Amer. Ceram. Soc.* **61** (1978) 271.
11. P. CHANTIKUL, B. R. LAWN and D. B. MARSHALL, *ibid.* in press.
12. B. R. LAWN and D. B. MARSHALL, *ibid.* **62** (1979) 106.
13. J. R. ROARK, "Formulas for Stress and Strain" (McGraw-Hill, New York and London, 1965) Chapter 10.
14. B. R. LAWN and D. B. MARSHALL, *Phys. Chem. Glasses* **18** (1977) 7.
15. S. M. WIEDERHORN, H. JOHNSON, A. M. DINESS and A. H. HEUER, *J. Amer. Ceram. Soc.* **57** (1974) 336.
16. P. CHANTIKUL, D. B. MARSHALL and B. R. LAWN, *ibid.* **61** (1979) 418.
17. H. P. KIRCHNER and R. M. GRUVER, *Mater. Sci. Eng.* **28** (1977) 249.
18. *Idem, ibid.* **34** (1978) 25.
19. H. P. KIRCHNER, *J. Amer. Ceram. Soc.* **61** (1978) 161.
20. M. V. SWAIN, *J. Mater. Sci.* **11** (1976) 2345.


Received 5 December 1978 and accepted 15 January 1979.